Accepted Manuscript

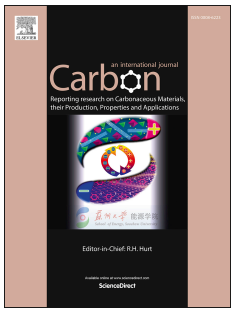

Super-sieving effect in phenol adsorption from aqueous solutions on nanoporous carbon beads

Piotr Kowalczyk, Artur Deditius, Wendell P. Ela, Marek Wiśniewski, Piotr A. Gauden, Artur P. Terzyk, Sylwester Furmaniak, Jerzy Włoch, Katsumi Kaneko, Alexander V. Neimark

PII: S0008-6223(18)30315-4

DOI: 10.1016/j.carbon.2018.03.063

Reference: CARBON 13006

To appear in: *Carbon*

Received Date: 20 November 2017

Revised Date: 18 March 2018

Accepted Date: 20 March 2018

Please cite this article as: P. Kowalczyk, A. Deditius, W.P. Ela, M. Wiśniewski, P.A. Gauden, A.P. Terzyk, S. Furmaniak, J. Włoch, K. Kaneko, A.V. Neimark, Super-sieving effect in phenol adsorption from aqueous solutions on nanoporous carbon beads, *Carbon* (2018), doi: 10.1016/j.carbon.2018.03.063.

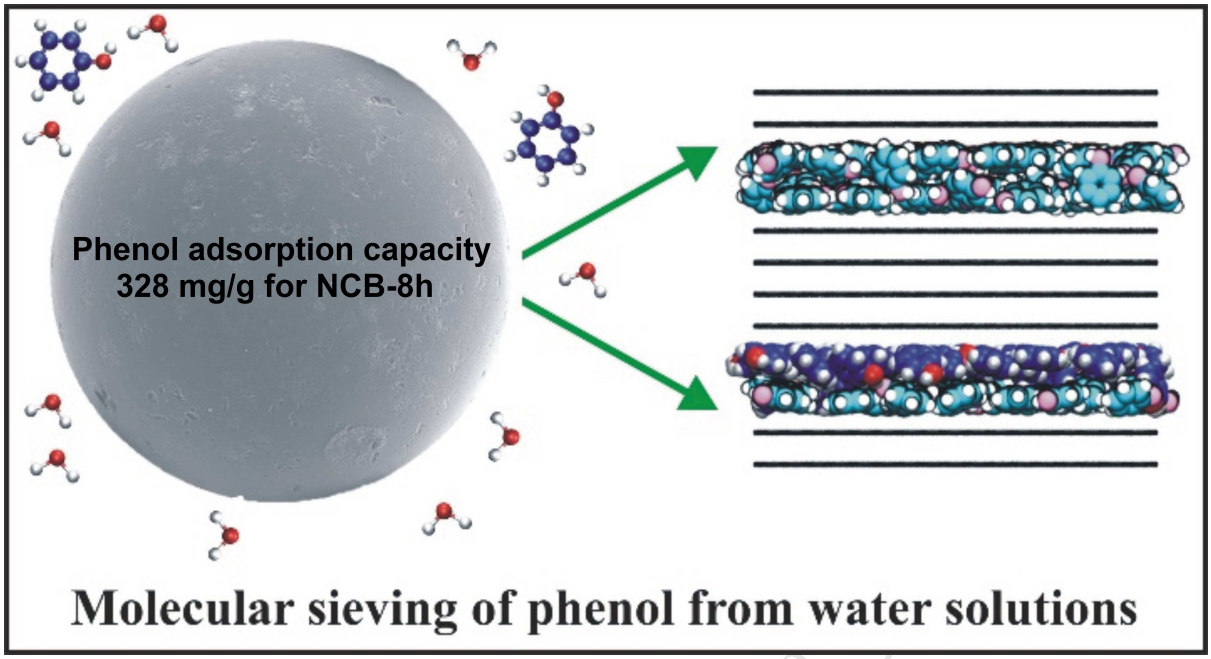

Super-sieving effect in phenol adsorption from aqueous solutions on nanoporous carbon beads

Piotr Kowalczyk[*1], Artur Deditius[1], Wendell P. Ela[1], Marek Wiśniewski[2], Piotr A. Gauden[2], Artur P. Terzyk[2], Sylwester Furmaniak[3], Jerzy Włoch[4], Katsumi Kaneko[5], and Alexander V. Neimark[6]

[1]School of Engineering and Information Technology, Murdoch University, 90 South Street, Murdoch 6150, Western Australia, Australia

[2]Faculty of Chemistry, Physicochemistry of Carbon Materials Research Group, Nicolaus Copernicus University in Toruń, Gagarin St. 7, 87-100 Toruń, Poland

[3]Stanisław Staszic University of Applied Sciences in Piła, 10 Podchorążych St., 64-620 Piła, Poland

[4]Faculty of Chemistry, Synthesis and Modification of Carbon Materials Research Group, Nicolaus Copernicus University in Toruń, Gagarin Street 7, 87-100, Toruń, Poland

[5]Center for Energy and Environmental Science, Shinshu University, Nagano, 380-8553, Japan

[6]Department of Chemical and Biochemical Engineering, Rutgers, The State University of New Jersey, 98 Brett Road, Piscataway, New Jersey 08854-8058, United States

Corresponding author. Tel: +61 8 9360 6936. Email: P.Kowalczyk@murdoch.edu.au (Piotr Kowalczyk)

Abstract

Removal of aromatic contaminants, like phenol, from water can be efficiently achieved by preferential adsorption on porous carbons which exhibit molecular sieving properties. Here, we present nanoporous carbon beads exhibiting an outstanding sieving effect in phenol adsorption from aqueous solution at neutral pH, which is evidenced experimentally and theoretically. The molecular sieving with pure phenol adsorbed phase is achieved by tuning the pore size and surface chemistry of the adsorbent. This study elucidates the essential role of hydrophobic interactions in narrow carbon micropores in removal and clean-up of water from organic pollutants. Furthermore, we suggest a new theoretical approach for evaluation of phenol adsorption capacity that is based on the Monte Carlo simulation of phenol adsorption with the relevance to the pore size distribution function determined by the density functional theory method from low temperature nitrogen adsorption.

1. Introduction

Phenol is a planar molecule with a hydroxyl group attached to the benzene ring. It represents a spectrum of toxic aromatic water contaminants characterized by limited solubility in aqueous solutions. In the last decade, there has been a considerable progress in the understanding of the mechanisms of phenol adsorption from aqueous solutions on carbonaceous nanomaterials at various pH [1-8]. However, these experimental studies lack a molecular level description of the adsorption processes in carbon pores. Furthermore, the theoretical characterization of the experimental measurements and postulated microscopic mechanisms of phenol adsorption from aqueous solutions relay on the classical methods of phenomenological thermodynamics, e.g. Dubinin's theory of micropore filling, Langmuir theory of adsorption at the solution/solid interface, general integral equation of adsorption, ideal solution theory, amongst others [1-10]. Although these theoretical approaches have provided valuable insights, their approximate nature may obscure the details of the phenol adsorption and/or water co-adsorption in pores of molecular size. The homogenous representation of adsorbed phases by classical thermodynamics is questionable, when the sizes of pores and adsorbed molecules are similar. This is because of the molecular packing effects in confining geometries [11,12].

Generally, it is believed that adsorption of phenol from aqueous solutions on carbon nanomaterials depends on fine-tuning of pore size and the control of the pore-wall chemistry [13-16]. Specific hydrogen bonding is believed to be responsible for a strong adsorption of water and phenol molecules on the primary adsorption sites, such as oxygen-containing functional groups dispersed around graphic edges and pore-wall defects [17,18]. Water and phenol molecules can also interact with common carbon impurities, e.g. metal oxides, silicates, aluminosilicates, heteroatoms, and others [9]. As a result, clusters of physisorbed water or/and phenol molecules around pore entrances and impurities may induce blocking of pore entrances, which potentially create excluded volumes in the pore network. Various impurities, defects, surface functional groups and dissolved oxygen can also catalyse the irreversible polymerisation of phenol molecules on graphic pore-walls [19-21]. Indeed, experiments have revealed that structural parameters (i.e., adsorption capacity, accessible surface area, micropore volume, and others) computed from phenol adsorption isotherms measured from aqueous solutions are underestimated in

comparison to those measured from gas phases. Kinetic factors, polymerisation and co-adsorption of water in carbon nanopores, has been used to explain lower uptake of phenol measured from aqueous solutions. However, as we pointed out, structural characteristics computed using methods of classical phenomenological thermodynamics only approximate this phenomenon and their use for postulation of the microscopic mechanism of phenol adsorption from aqueous solutions in narrow slit-shaped carbon pores, with pore width < 2 nm, is controversial [9,11,12].

Following the theory of hydrophobic effect developed by Chandler et al. [22-25], it is expected that narrow slit-shaped graphitic carbon pores, classified as micropores with pore width < 2 nm [26], can induce molecular sieving of aromatic molecules from aqueous solutions at neural pH. This is because the transfer of water molecules from aqueous solutions to hydrophobic micropores (i.e., between extended graphitic pore walls with separation < 2 nm) is thermodynamically unfavorable [27-30]. However, planar molecules with benzene-ring motif can be adsorbed in slit-shaped carbon micropores through London dispersion and hydrophobic interactions [31]. In this paper we provide a combine experimental and theoretical evidence that micropores of nanoporous carbon beads are filled with pure phenol at saturation, leading to selective molecular sieving of phenol from aqueous solutions at neutral pH and 298 K.

2. Experimental

2.1 Synthesis

Samples of nanoporous carbon beads (NCB) were prepared by carbonization of acidic, gel-type cation exchange resin based on a styrene-divinylbenzene copolymer (Lanxess Lewatit, Germany) and subsequent activation with CO_2 at Murdoch University. In a carbonization step, ~2 g of precursor were placed in a ceramic crucible and carbonized at 650 ^oC for 1.5 hours in a high-purity N_2 steam (~1.0 dm^3/ min, BOC, Australia) in a horizontal split-tube furnace. In a second step, the carbonized beads were activated with CO_2 at 900 ^oC for 1, 3, 5, and 8 hours in a high-purity CO_2 steam (~1.0 dm^3/min, BOC, Australia) in a horizontal split-tube furnace. The resulting carbon samples were labelled NCB-xh, where x denotes the CO_2 activation time in hours (e.g., x is 1, 3, 5 and 8).

2.2 Characterization

Raman spectra of NCB samples were recorded using the WITec alpha 300RA+ confocal Raman imaging system at the Centre for Microscopy, Characterisation and Analysis (CMCA), The University of Western Australia (UWA). We used the laser excitation wavelength of 532 nm. For each carbon sample, Raman spectra were collected from ~4-6 points chosen randomly on the surface of NCB sample. Raman D- (1350 cm^{-1}) and G-band (1580 cm^{-1}) was fitted using double Lorentzian model [32,33]. In-plane sizes of graphitic crystallites were estimated from the Ferrari-Robertson equation [34]. The N_2 adsorption-desorption isotherms on NCB samples were measured at 77 K using the ASAP 2010 MicroPore System (Micromeritics, USA) at Nicolaus Copernicus University. Before each measurement, the carbon samples were desorbed in vacuum at 383 K for 3 h [35]. Adsorption and structural parameters of NCB samples were computed using Brunauer-Emmett-Teller (BET) theory of multilayer adsorption [36], and general integral equation of adsorption implemented with local N_2 adsorption isotherms computed from classical non-local density functional theory (NLDFT) and quenched solid density functional theory (QSDFT) [37,38]. X-ray powder scattering patterns (XRD) of NCB samples were recorded using the Empyrean multi-purpose research diffractometer using Cu Kα radiation (λ = 0.15406 nm) at CMCA, UWA. Scanning electron microscope images (SEM) and the energy-dispersive X-ray (EDX) spectra of NCB samples were recorded using the Verios XHR SEM system at the CMCA, UWA. The average spacing between graphitic layers in all studied NCB samples was computed from Bragg equation [39]. The enthalpy of immersion of NCB samples in water and in phenol solutions was measured at T = 298 K (or at 298, 303, and 308 K for NCB-1h sample) using a Tian-Calvet isothermal microcalorimeter constructed in physicochemistry of carbon materials research group at Nicolaus Copernicus University, following the procedure described previously [40,41]. The measurement for each NCB sample was repeated three times. The error was not larger than 0.5 mJ/m^2. Quantitative analyses of adsorption isotherms were determined using UV-Vis spectrophotometer JASCO V-660 by the analysis of equilibrium concentration (after 48h equilibration) measured at 270 nm [40,41].

3. Results and Discussion

Figure 1a,c present scanning electron microscopy (SEM) images of the surface of NCB-8h sample (SEM images of all remaining NCB samples are displayed in Fig. 1S,2S in the Supporting Information). The microscopic observations show that with increasing activation time, the surface area covered by patches of pore entrances on NCB increases. For NCB-8h, pore entrances cover the entire surface of spherical, ~400 μm in diameter, carbon bead. The high magnification SEM image of the NCB-8h surface (Fig. 1c) shows a sponge-like carbon with pore entrances ~<2 nm, which suggests that micropores formed during CO_2 activation tend to be directly connected to the exterior. The Raman spectral examination of the material display two overlapping broad bands locating at ~1350 and ~1590 cm^{-1} (Fig. 1b). Such feature is associated with the disordering of the samples (D band) and stretching vibration in the aromatic planes (G band), respectively [42,43]. These two bands originate from the nanometer-scale graphitic crystallites [42,43]. The in-plane size of graphitic crystallites, ~2.1-2.4 nm, computed from the Ferrari-Robertson equation [34] is similar to all NCB samples (Table 1).

Sample	L_a (nm)	d_{002} (nm)
NCB-1h	2.3	0.388
NCB-3h	2.4	0.397
NCB-5h	2.1	0.399
NCB-8h	2.2	0.399

Table 1. Crystallographic and crystallite parameters estimated from confocal Raman and XRD measurements.

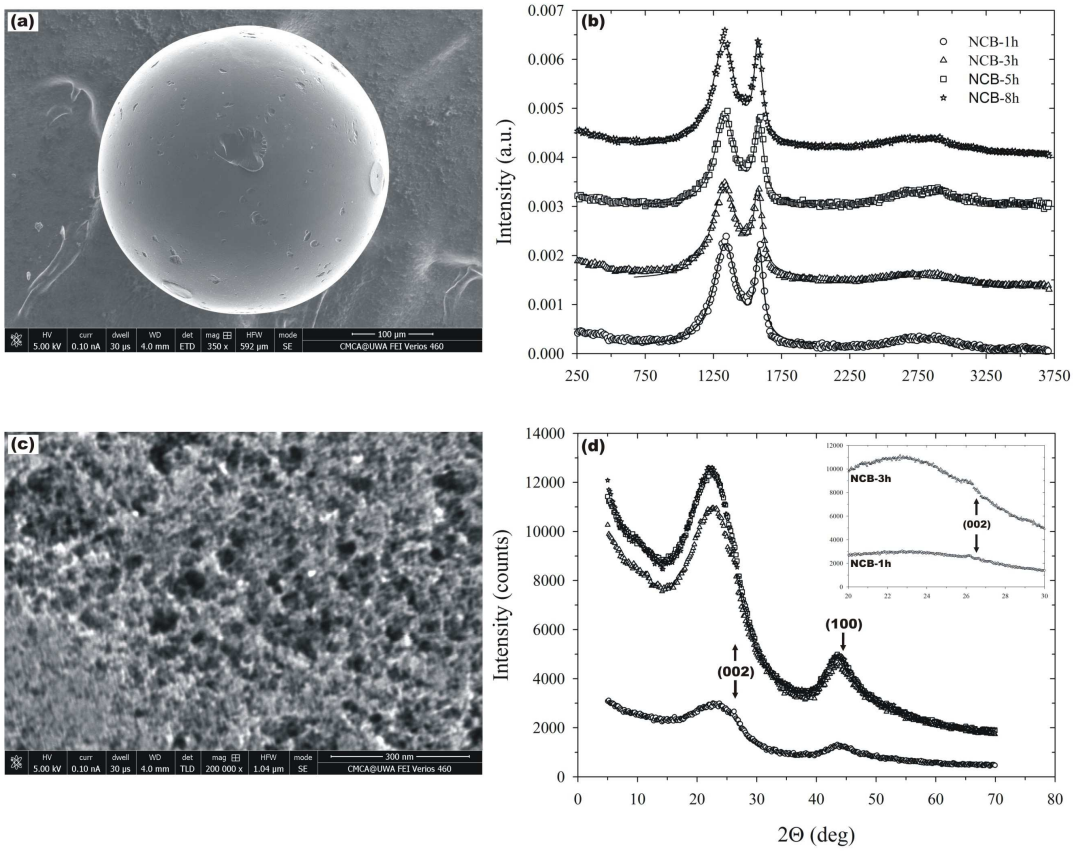

Figure 1. (a) SEM image of the NCB-8h sample activated using CO_2 at 900 ^oC for 8 hours. (b) Experimental (symbols) and deconvoluted (solid lines) Raman spectra of NCB samples activated using different CO_2 activation time (NCB-xh, where xh denotes activation time in hours). (c) High magnification SEM image of the surface of the NCB-8h showing pore entrances. (d) XRD diffraction patterns for NCB (symbols) with spectral (002) and (100) diffraction peaks corresponding to graphite. Insert panel highlights a low intensity (002) diffraction peak found on XRD diffraction patterns recorded for NCB-1h and NCB-3h samples only.

X-ray diffraction (XRD) patterns shown on Figure 1d are dominated by intensities of (002) and (100) peaks. The (002) diffraction peaks are broadened and shifted to lower angles as compared to (002) diffraction peak of graphite, which indicates larger interlayer spacing between graphitic planes of nano-crystallites than those of graphite [44]. Indeed, an average interlayer spacing (d002) computed for all NCB samples is greater than this of graphite spacing of 0.335 nm (Table 1). These structural characteristics are typical for turbostratic carbonaceous materials [44-46].

Therefore, a graphitic slit-shaped pore model was used for pore size distribution analysis and computer modelling of phenol adsorption in NCB samples [47-50].

The composition of phenol-water mixtures adsorbed in graphitic micropores embedded in disordered carbon matrix is not directly measurable. However, if the water co-adsorption in micropores is negligible, it may be expected that the theoretical phenol-saturated capacity of NCB sample is comparable with the experimentally measured saturation capacity of phenol from aqueous solutions at neutral pH. This assumption is justified for Langmuir type adsorption isotherm (e.g. type L isotherm following to Gilles classification) measured from aqueous solutions only, when the affinity of solute to adsorbent is very high [51,52].

To calculate the phenol-saturated capacity of NCB samples, $N_{sat.}$, we propose a novel two-step approach. In the first step, we performed constant pressure Gibbs ensemble Monte Carlo simulations (CP-GMC) of pure phenol adsorption in graphitic slit-shaped pores at saturated vapor pressure of phenol and 301 K (Section 1 in the Supporting Information) [53,54]. This allowed us to determine the pore-size dependence of phenol-saturated capacity, $N_{theor.}(H)$, computed as the adsorbed mass of pure phenol per unit area of pore walls, in the entire range of micropores accessible to phenol molecules (0.23 nm < H < 2.0 nm). In a second step, for each NCB sample, we determined the pore size distribution function, f(H), from the experimental N_2 adsorption isotherm (77 K), $N_{expt.}(p/p_0)$, by deconvolution of the generalized adsorption equation using second-order Tikhonov regularization functional with non-negativity constrain given by the following expression [55-57]:

$$N_{expt.}(p/p_0) = \int N_{NLDFT}(p/p_0, H) f(H) dH \quad (1)$$

The set of local N_2 adsorption isotherms in slit-shaped graphitic nanopores, $N_{NLDFT}(p/p_0,H)$, were generated from the non-local density functional theory proposed by Tarazona (Section 2 in the Supporting Information).

Having a pore size distribution function and the pore-size dependence of phenol-saturated capacity, we predicted theoretically the phenol-saturated capacity for each NCB sample by using the following expression:

$$N_{sat.} = \int N_{theor.}(H) f(H) dH \quad (2)$$

Note that in eq. (1) it is assumed that carbon micropores filled with N_2 molecules at 77 K are fully accessible to phenol molecules adsorbed from aqueous solutions at neutral pH and 298 K. The experimental verification of this assumption is presented in Figure 7d.

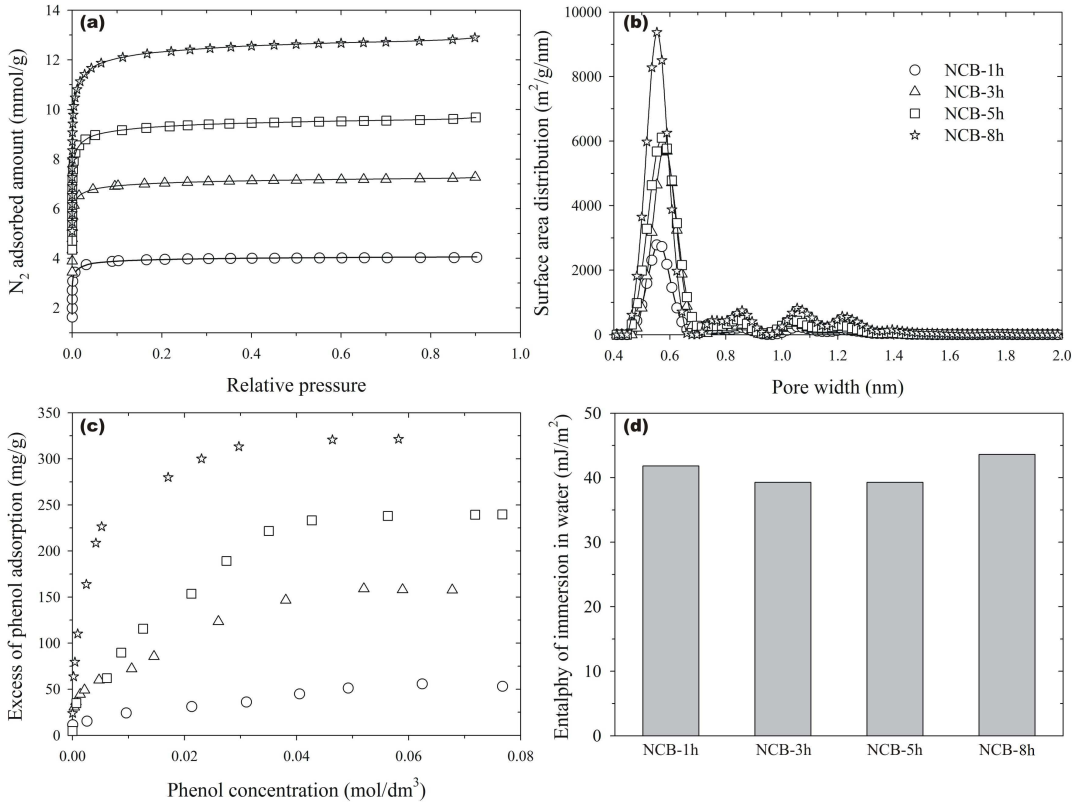

Figure 2. (a) Experimental N_2 adsorption isotherms (77 K) on series of NCB samples (solid lines presents NLDFT fitting). (b) Pore size distributions functions computed from N_2 adsorption isotherms and NLDFT method. (c) Experimental phenol adsorption isotherms from aqueous solutions at neutral pH (298 K). (d) Experimental enthalpy of NCB immersion in water per surface area measured at 298 K.

Figure 2a presents the N_2 adsorption isotherms on NCB at 77 K measured volumetrically. The isotherms are typical for microporous materials with graphitic pores of uniform size (type I isotherm following to IUPAC) [26]. The surface area of micropore walls and micropore volume of NCB is fine-tuned by CO_2 activation time (Table 2). For all synthetised NCB samples, a dominant contribution from graphitic

ultramicropores (pore width < 0.6 nm) is shown by NLDFT pore size distribution functions (Fig. 2b). In addition, the NCB-5h and NCB-8h samples contain a fraction of graphitic supermicropores (0.6 < pore width < 2.0). Figure 2c,d illustrate the impact of CO_2 activation time on the adsorption of phenol from aqueous solutions at neutral pH and the enthalpy of NCB immersion in water solutions, respectively. Adsorption of phenol from water solutions on NCB samples is very sensitive to small variations in a pore-size distribution function. Sample NCB-1h adsorbs only ~50 mg/g of phenol at 0.08 mol/dm^3 and the plateau is not experimentally reached (Fig. 2c). The pore structure of NCB-3h, -5h and -8h is then progressively opened with a longer CO_2 activation time. This phenomenon explains a gradual transformation of a linear phenol adsorption isotherm (sample NCB-1h) to the Langmuir type isotherm measured for NCB-8h sample. The phenol adsorption capacity of 322 mg/g measured for NCB-8h is one of the highest reported for a spectrum of adsorbents (Fig. 3). In contrast, measured enthalpy of immersion of studied carbon samples in water shows little variation between studied carbon samples and it ranges from 39-42 mJ/m^2 (Fig. 2d). Therefore, it implies that during the progressive activation of carbonized polymer beads there are no changes in the chemical composition of carbon surface. Moreover, the comparison of immersion enthalpies of NCB in water with the calorimetric data published for chemically modified activated carbons leads to the conclusion about negligibly small concentration of surface functional groups [40]. The results of energy-dispersive X-ray spectroscopy (EDX) analysis confirm that all NCB samples contain mostly carbon (~90 %), sulfur (~6%), and oxygen (~4%) (Fig. 3S-6S in the Supporting Information).

Sample	S_{BET} (m^2/g)	S_{NLDFT} (m^2/g)	S_{QSDFT} (m^2/g)	a_{BET} (mmol/g)	$a_{expt.}$ (mmol/g)	v_{QSDFT} (cm^3/g)
NCB-1h	274	380	386	2.8	4.0	0.13
NCB-3h	484	687	728	5.0	7.3	0.23
NCB-5h	661	905	954	6.8	9.7	0.31
NCB-8h	902	1186	1194	9.2	13.0	0.41

Table 2. Nanopore parameters estimated from N_2 adsorption isotherms at 77 K.

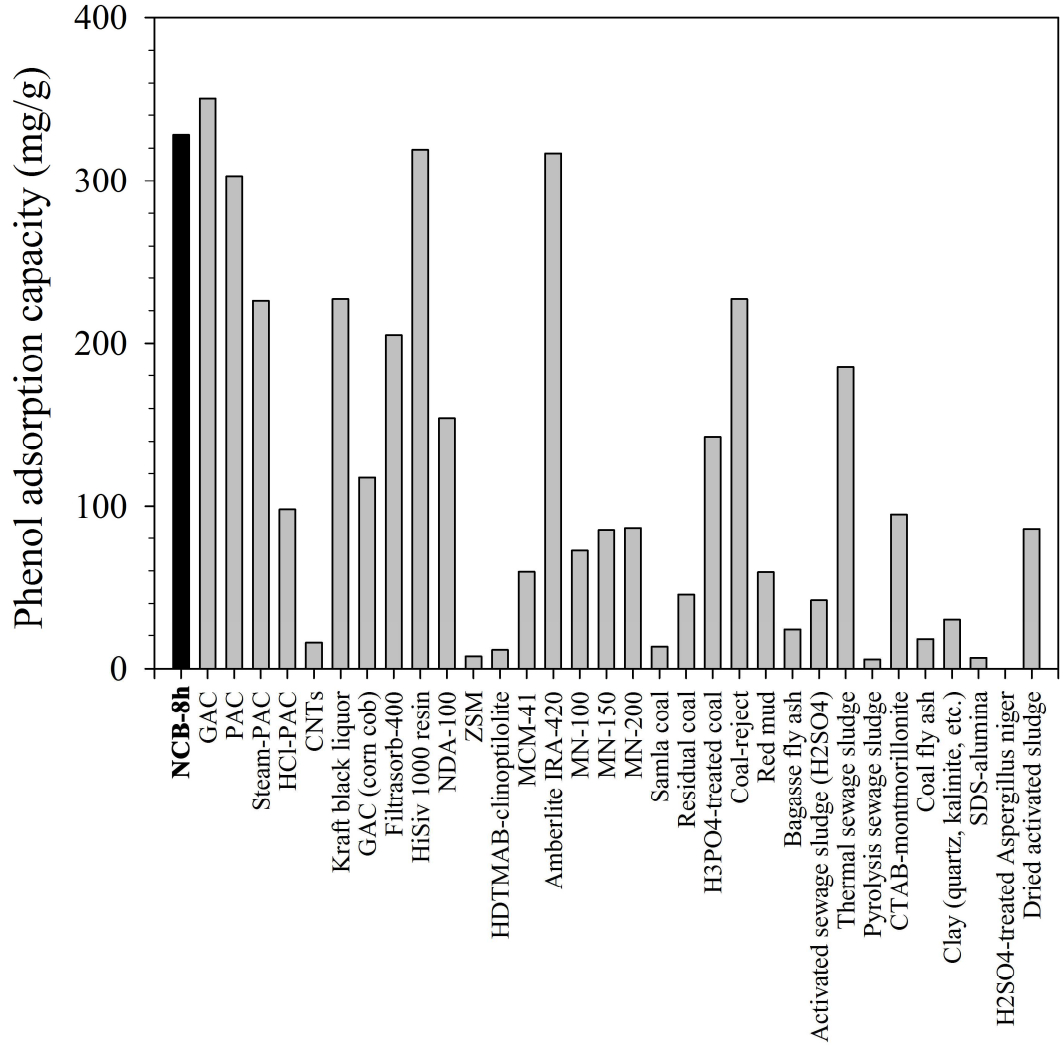

Figure 3. Evaluation of the best adsorbents for phenol removal [58]. The NCB-8h sample was synthetised in the current study.

In equilibrium-controlled adsorption, planar phenol molecules are able to adsorb in extremely narrow ~0.28 nm ultramicropores. The phenol-saturated capacity computed per surface area of graphic pore walls increases linearly with pore width, with an exception of singe- to double-layer packing transition around ~0.6 nm (Fig. 4). The number of hydrogen bonds (H-bonds) per phenol molecule in slit-shaped pores saturated with pure phenol depends on the pore width (Fig. 5 and movies in the Supplemental Information). In narrow carbon ultramicropores <0.6 nm, graphitic pore-walls imposed strong constraints for rotations of phenol molecules (Fig. 6). Phenol molecules adsorbed in ~0.3-0.42 nm ultramicropores are lying flat on

graphitic pore-walls, and the structure of the adsorbed film is stabilized by ~1.0-1.1 H-bonds per phenol molecule. With widening of pore, an increase in orientation disorder and a decrease in a number of H-bonds (Fig. 5,6) is observed. A clear minimum of ~0.8 H-bonds per phenol molecule (i.e. liquid-like phenol) corresponds to a single- to double-layer packing transition of the adsorbed phenol (Fig. 4).

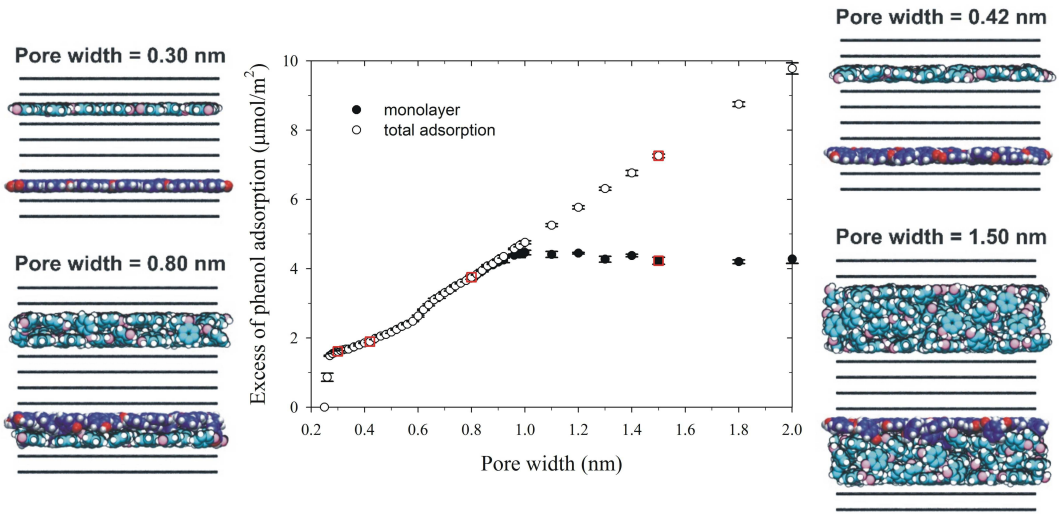

Figure 4. Pore-width dependence of pure phenol adsorption capacity (open circles) in graphitic slit-shaped pores computed from CP-GMC simulations (301 K, 59 Pa). The contribution from the monolayer capacity is displayed by filled circles. Snapshots on the left- and right-hand side of the plot show packing of phenol at saturation in 0.3, 0.42, 0.8, and 1.5 nm micropores (red squares in the middle panel). Note that the graphics collected in this figure, and Fig. 5,6 are created using the VMD program [59].

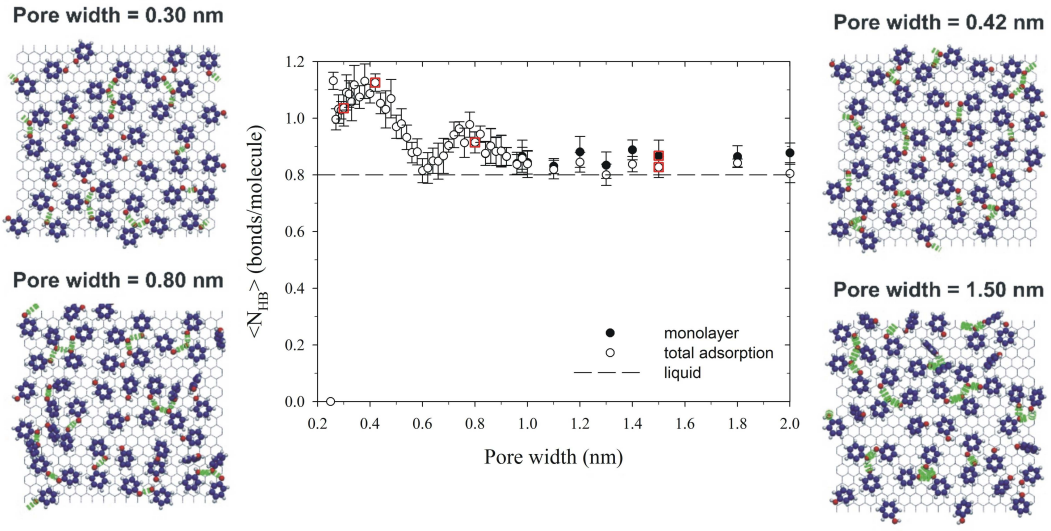

Figure 5. Variation of the number of H-bonds per phenol molecule vs. pore-width in contact layers (black circles) and in the entire adsorbed phases (open circles) computed from CP-GMC simulations (301 K, 59 Pa). Dashed horizontal line corresponds to a number of H-bonds in liquid phenol. Snapshots on the left- and right-hand side of the plot show H-bonding between phenol molecules at the contact monolayer films in 0.3, 0.42, 0.8, and 1.5 nm micropores (red squares in the middle panel).

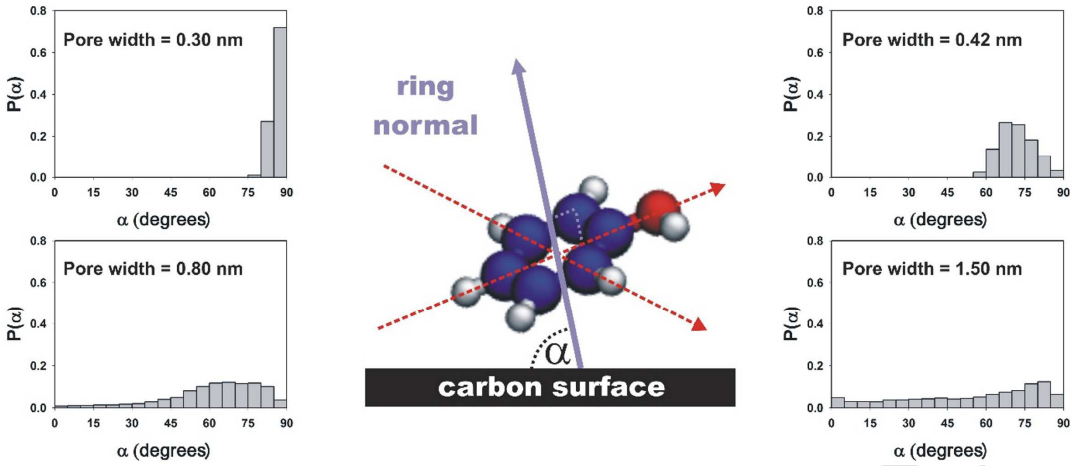

Figure 6. Histograms showing the angular orientations of the phenol molecules adsorbed in 0.3, 0.42, 0.8 and 1.5 nm slit-shaped graphitic pores.

The analysis of theoretical phenol-saturated capacity for the studied NCB samples clearly demonstrates the importance of pore-size distribution function in the entire range of micropores (Fig. 7a,b). The phenol-saturated capacity is dominated by contribution from graphitic ultramicropores <0.6 nm (Fig. 7a,b). This is because the surface area of the ultramicropore walls is significantly higher than the surface area of the supermicropore walls (Fig. 2b). During the CO_2 activation process, ultramicropores are created first. Subsequently, the fraction of supermicropores is developed by widening the existing ultramicropores. However, as it is shown in Figure 4, the values of phenol-saturated capacity in supermicropores are significantly higher compared to ultramicropores characterized by restricted adsorption space and close proximity of the pore walls. As a result, the phenol capacity per mass of NCB sample is steeply increasing up to ~0.6 nm, followed by its gradual increase up to ~1.4-1.6 nm (Fig. 7b).

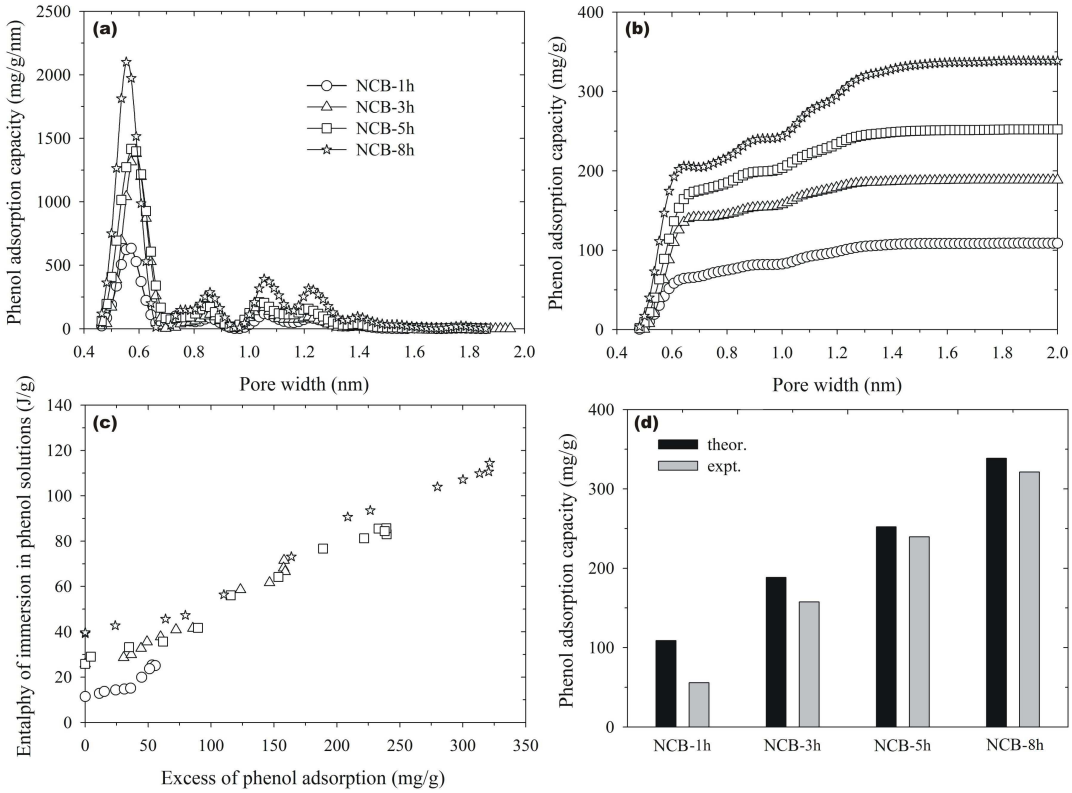

Figure 7. (a, b) Theoretical differential and cumulative phenol-saturated capacity of NCB computed from NLDFT pore size distributions (Fig. 2b) and phenol-saturated capacity simulated in graphic slit-shaped pores (Fig. 4). (c) Experimental enthalpy of NCB immersion in aqueous solutions of phenol at 298 K. (d) Theoretical and experimental capacity of phenol on NCB samples measured from aqueous solutions at neutral pH and 298 K.

The comparison between theoretical phenol-saturated capacity and the experimentally measured phenol capacity from aqueous solutions at neutral pH shows remarkable agreement for NCB-8h and NCB-5h (Fig. 7d, with an error of ~5%). Note that phenol adsorption isotherms measured for these samples are of Langmuir type, and the saturation of micropores is reached at ~0.04 mol/dm^3. Thus, it is concluded that NCB-5h and NCB-8h sample is saturated with a pure phenol, while the water molecules stay at solutions. The co-adsorption of water in carbon micropores is negligible because building of thin water films at the extended graphic pore walls is thermodynamically unfavorable, as is predicted by theory of hydrophobic hydration [22-25]. To the best of our knowledge, this is the first microscopic evidence of molecular sieving of phenol from aqueous solutions at neutral pH.

The adsorption of phenol from aqueous solutions in nanoporous carbon beads activated for three hours (NCB-3h) decreases to ~180 mg/g at saturation, which can be explained by its lower surface area of the micropore walls (Table 2). However, the experimental adsorption capacity of phenol from water solutions on NCB-3h is overestimated by the theoretical phenol-saturated capacity by ~20 mg/g. This result can be explained by poor accessibly of narrow ultramicropores for phenol molecules due to a short time of CO_2 activation. Analysis of phenol adsorption on NCB-1h reveals a significant overestimation of the experimental phenol adsorption capacity measured at 0.08 mmol/dm^3 by the theoretical phenol-saturated capacity by ~50 %. Such discrepancy is likely to be a result of out of thermodynamic equilibrium adsorption of phenol on NCB-1h sample from aqueous solutions at neural pH.

To confirm the hypothesis that adsorption of phenol from aqueous solutions on NCB-1h sample at neutral pH is a non-equilibrium process, we performed a set of adsorption and calorimetry measurements at higher temperatures. Figure 8a,d display the temperature variation of phenol adsorption from aqueous solutions on NCB-1h at neutral pH; supported by experimental values of the enthalpy of NCB-1h immersion in water and phenol solutions measured at 298, 303, and 308 K. The enthalpy of NCB-1h immersion in water, ~40-49 mJ/m^2, is relatively small and similar for different temperatures indicating that surface chemistry is not responsible for the anomalous adsorption of phenol on NCB-1h sample. The amount of the adsorbed phenol and the enthalpy of immersion in phenol solutions increases with temperature because the narrow carbon ultramicropores are more accessible to phenol at higher temperatures. Therefore, the adsorption of phenol from aqueous solutions on NCB-1h at neutral pH is controlled by slow diffusion of phenol molecules into micropores despite connection of the micropores with the exterior [6]. Furthermore, we noticed that saturation of the pore spaces has not been achieved within the timescale of the experiment at 308 K. Still, the amount of the adsorbed phenol measured at 0.08 mol/dm^3 increases with temperature and it is approaching the theoretical phenol-saturated capacity computed from pore size distribution function and pore-width dependence of pure phenol capacity (Fig. 7d,8d). The experimental results and proposed methodological development provide the evidence of molecular sieving of phenol from aqueous solutions at neutral pH in NCB samples with high degree of activation (e.g. NCB-5h and NCB-8h). In contrast, the adsorption of phenol from

water solutions at neutral pH on NCB-1h sample with low degree of activation of carbon precursor is out of thermodynamic equilibrium.

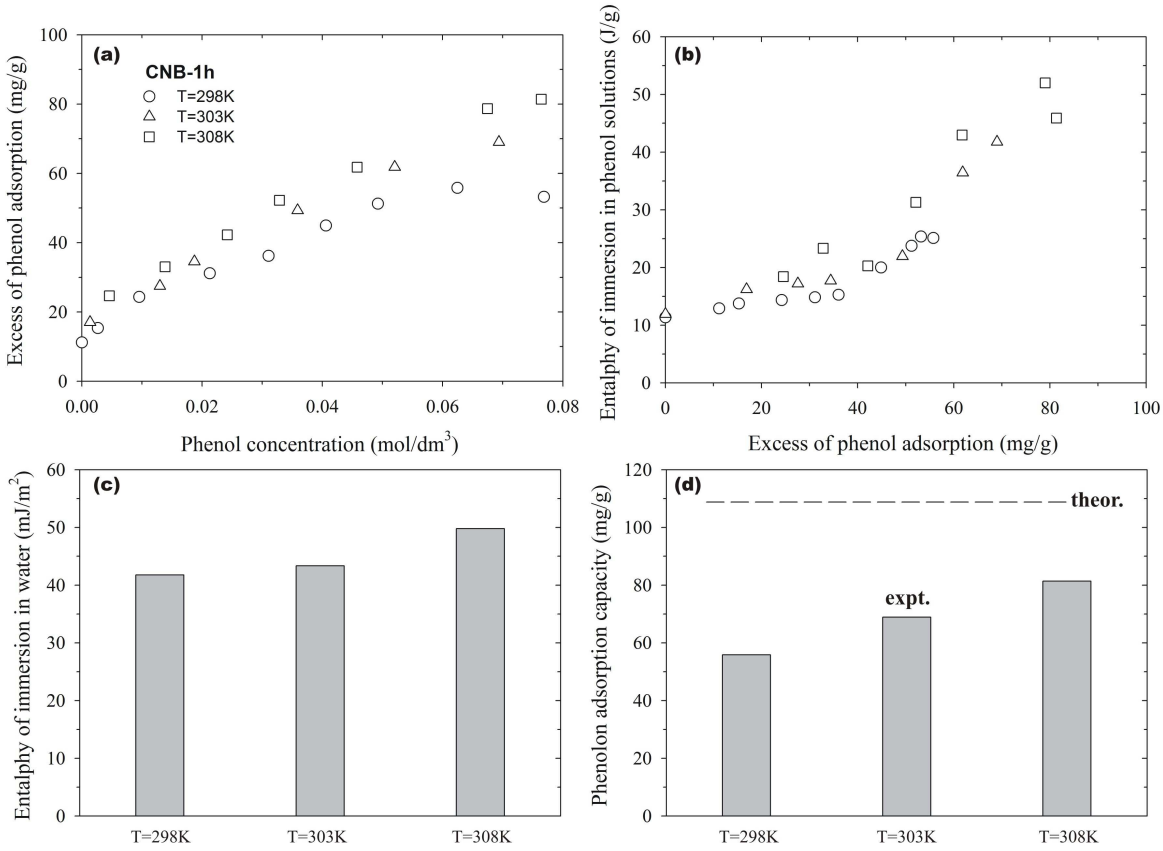

Figure 8. (a, b) Temperature-dependence of phenol adsorption and enthalpy of NCB-1h immersion in phenol solutions, respectively. (c) Temperature-dependence of the enthalpy of NCB-1h immersion in water. (d) Variation of the experimental phenol adsorption capacity (expt.) measured at 0.08 mol/dm^3 with temperature for NCB-1h. The theoretical phenol-saturated capacity of NCB-1h (theor. Fig. 7d) is given by vertical dashed line.

4. Conclusions

We report experimental results of phenol adsorption and immersion in water and phenol solutions on a series of nanoporous carbon beads (NCB) prepared from polymeric precursor at neutral pH and 298 K. Calorimetric measurements show that the enthalpy of immersion for all NCB samples in water is ~39-42 mJ/m^2 at 298 K, indicating that CO_2 activation time does not modify the surface chemistry of studied

nanoporous carbons. Low values of the enthalpy of immersion in water and EDX analysis confirm that all synthetised NCB samples are hydrophobic nanocarbons. NLDFT/QSDFT pore size analysis reveal that all carbon beads are strictly microporous materials with pore sizes < 1.4-1.6 nm. The turbostratic model of carbon micropores in NCB is confirmed by XRD and confocal Raman spectroscopy analysis. The mechanism of phenol adsorption is affected by a small variation in pore size distribution functions. NCB samples activated by using CO_2 for 5h and 8h at 900 ^oC show large adsorption of phenol from aqueous solutions with saturation of micropores at ~0.04 mol/dm^3. The best adsorbent NCB-8h adsorb 322 mg/g of phenol at saturation, which indicates that co-adsorption of water in this carbon sample is negligible. Indeed, theoretical value of 338 mg/g of phenol adsorption computed from the NLDFT pore size distribution and pore-width dependence of pure phenol density in NCB-8h micropores is consistent with the mechanism of molecular sieving with pure phenol adsorbed phase. For NCB-5h sample, the experimental and theoretical saturation uptake of phenol is 230 and 252 mg/g, respectively. Therefore, experiment and theory consistently show that the co-adsorption of water in NCB-8h and NCB-5h samples is negligible. Theory of hydrophobic hydration at extended hydrophobic surfaces postulate the mechanism of phenol sieving from water at the neutral pH. This theory is also consistent with the experimental measurements of phenol adsorption on graphitized carbon black. Király et al. [60] showed that the experimental enthalpy of phenol adsorption on graphitized carbon black in the first layer (-11.3 kJ/mol) is close to the value of the enthalpy of fusion of 11.514 kJ/mol for phenol at 314.06 K [61]. This indicates that the contact layer of phenol adsorbed on graphite is solid-like, and the co-adsorption of water is negligible. In next adsorbed layer the enthalpy of phenol adsorption is not so exothermic showing that the molecules are more mobile. Our theoretical and experimental results showed that solid-like phenol is stabilized in the entire adsorption space of micropores by confinement effects. The experimental uptake of phenol in NCB-3h and NCB-1h measured at 0.08 mol/dm^3 is overestimated by the theory. The phenol adsorption and calorimetry measurements on NCB-1h at higher temperatures show that adsorption process is out of thermodynamic equilibrium.

Taking into account that carbon surface oxidation leads to decrease in phenol adsorption, the unmodified carbons should be applied to obtain satisfactory phenol uptake from aqueous solutions. In this case, knowing the pore size distribution

function calculated from low-temperature N_2 adsorption isotherm, and using the approach proposed in this study, one can estimate maximum phenol adsorption capacity. This is the most important practical application of our approach that can be used for in-silico designing of carbon adsorbents for removal and clean-up of water from phenol. The application of this approach for the study of adsorption of other non-electrolyte water pollutions will be reported in future.

Acknowledgements

P. K. acknowledges the financial support from the Murdoch University start-up grant: Nanopore controlled synthetic carbons for interfacial separations and catalysis (11701). P. K. and A. D. gratefully acknowledges Dr. T. Becker (Curtin University) for his assistance with confocal Raman measurements.

Appendix A. Supplementary Data

Supplementary data associated with this article can be found, in the online version.

References

[1] A. Dabrowski, P. Podkościelny, Z. Hubicki, M. Barczak, Adsorption of phenolic compounds by activated carbon-a critical review, Chemosphere 58 (2005) 1049-1070.

[2] E. Fernandez, D. Hugi-Cleary, M. V. Lopez-Ramon, F. Stoeckli, Adsorption of phenol from dilute and concentrated aqueous solutions by activated carbons, Langmuir 19 (2003) 9719-9723.

[3] C. T. Hsieh, H. Teng, Liquid-phase adsorption of phenol onto activated carbons prepared with different activation levels, J. Coll. Interf. Sci. 230 (2000) 171-175.

[4] C. Moreno-Castilla, Adsorption of organic molecules from aqueous solutions on carbon materials, Carbon 42 (2004) 83-94.

[5] D. M. Nevskaia, A. Santianes, V. Munoz, A. Guerrero-Ruiz, Interaction of aqueous solutions of phenol with commercial activated carbons: an adsorption and kinetic study, Carbon 37 (1999) 1065-1074.

[6] F. Caturla, J. M. Martin-Martinez, M. Molina-Sabio, F. Rodriguez-Reinoso, R.

Torregrosa, Adsorption of substituted phenols on activated carbon, J. Coll. Interf. Sci. (124) 1988 528-534.

[7] K. Laszlo, Adsorption from aqueous phenol and aniline solutions on activated carbons with different surface chemistry, Coll. & Surf. A: Physicochem. Eng. Aspects 265 (2005) 32-39.

[8] L. R. Radovic, C. Moreno-Castilla, J. Rivera-Utrilla, in Chemistry and Physics of Carbon, L. R. Radovic, editor , Vol. 27, Chapter 4, New York: Marcel Dekker, 2001.

[9] R. C. Bansal, M. Goyal, Activated carbon adsorption, Boca Raton: CRC Press, 2005.

[10] K. Laszlo, P. Podkościelny, A. Dabrowski, Heterogeneity of polymer-based active carbons in adsorption of aqueous solutions of phenol and 2,3,4-trichlorophenol, Langmuir 19 (2003) 5287-5294.

[11] A. V. Neimark, P. I. Ravikovitch, A. Vishnyakov, Bridging scales from molecular simulations to classical thermodynamics: density functional theory of capillary condensation in nanopores, J. Phys.: Condens. Matter 15 (2003) 347-365.

[12] P. Tarazona, U. M. B. Marconi, R. Evans, Phase equilibria of fluid interfaces and confined fluids: non-local versus local density functionals, Mol. Phys. 60 (1987) 573-595.

[13] I. I. Salame, T. J. Bandosz, Role of surface chemistry in adsorption of phenol on activated carbons, J. Coll. Interf. Sci. 264 (2003) 307-312.

[14] F. Stoeckli, M. V. Lopez-Ramon, C. Moreno-Castilla, Adsorption of phenolic compounds from aqueous solutions, by activated carbons, described by the Dubinin-Astakhov equation, Langmuir 17 (2001) 3301-3306.

[15] R. W. Coughlin, F. S. Ezra, Role of surface acidity in the adsorption of organic pollutants on the surface of carbon, Environ. Sci. Technol. 2 (1968) 291-297.

[16] T. J. Bandosz, Activated carbon surfaces in environmental remediation, Vol. 7, Oxford: Elsevier, 2006.

[17] A. P. Terzyk, P. A. Gauden, S. Furmaniak, R. P. Wesolowski, P. J. F. Harris, Molecular dynamics simulation insight into the mechanism of phenol adsorption at low coverages from aqueous solutions on microporous carbons, Phys. Chem. Chem. Phys. 12 (2010) 812-817.

[18] F. Stoeckli, D. Hugi-Cleary, On the mechanisms of phenol adsorption by carbons, Russ. Chem. Bull. 50 (2001) 2060-2063.

[19] T. M. Grant, C. J. King, Mechanism of irreversible adsorption of phenolic compounds by activated carbons, Ind. Eng. Chem. Res. 29 (1990) 264-271.

[20] A. P. Terzyk, Further insights into the role of carbon surface functionalities in the mechanism of phenol adsorption, J. Coll. Interf. Sci. 268 (2003) 301-329.

[21] A. P. Terzyk, The impact of carbon surface chemical composition on the adsorption of phenol determined at the real oxic and anoxic conditions, Appl. Surf. Sci. 253 (2007) 5752-5755.

[22] D. Chandler, Interfaces and the driving force of hydrophobic assembly, Nature 437 (2005) 640-647.

[23] K. Lum, D. Chandler, J. D. Weeks, Hydrophobicity at small and large length scales, J. Phys. Chem. B 103 (1999) 4570-4577.

[24] D. Chandler, Hydrophobicity: two faces of water, Nature 417 (2002) 491.

[25] T. F. Miller III, E. Vanden-Eijnden, D. Chandler, Solvent coarse-graining and the string method applied to the hydrophobic collapse of a hydrated chain, Proc. Natl. Acad. Sci. 104 (2007) 14559-14562.

[26] M. Thommes, K. Kaneko, A. V. Neimark, J. P. Olivier, F. Rodriguez-Reinoso, J. Rouquérol et al., Physisorption of gases, with special reference to the evaluation of surface area and pore size distribution (IUPAC Technical Report), Pure Appl. Chem. 87 (2015) 1051-1069.

[27] K. Leung, A. Luzar, D. Bratko, Dynamics of capillary drying in water, Phys. Rev. Lett. 90 (2003) 0655902-1.

[28] A. Luzar, Activation barrier scaling for the spontaneous evaporation of confined water, J. Phys. Chem. B 108 (2004) 19859-19866.

[29] P. R. ten Wolde, Hydrophobic interactions: an overview, J. Phys.: Condens. Matter 14 (2002) 9445-9460.

[30] T. R. Jensen, M. O. Jensen, N. Reitzel, K. Balashev, G. H. Peters, K. Kjaer et al. Water in contact with extended hydrophobic surfaces: direct evidence of weak dewetting, Phys. Rev. Lett. 90 (2003) 086101-1.

[31] J. N. Israelachvili, Intermolecular and Surface Forces, Oxford: Academic Press 2011.

[32] R. Storn, K. Price, Differential evolution - a simple and efficient heuristic for global optimization over continuous spaces, J. Glob. Optim. 11 (1997) 341-359.

[33] S. Furmaniak, P. A. Gauden, A. P. Terzyk, G. Rychlicki, Water adsorption on

carbons - critical review of the most popular analytical approaches, Adv. Colloid. Interface Sci. 137 (2008) 82-143.

[34] A. C. Ferrari, J. Robertson, Interpretation of Raman spectra of disordered and amorphous carbon, Phys. Rev. B 61 (2000) 14095-14107.

[35] A. P. Terzyk, P. A. Gauden, J. Zawadzki, G. Rychlicki, M. Wisniewski, P. Kowalczyk, Toward the characterization of microporosity of carbonaceous films, J. Coll. Interface Sci. 243 (2001) 183-192.

[36] S. Brunauer, P. H. Emmett, E. Teller, Adsorption of gases in multimolecular layers, J. Am. Chem. Soc. 60 (1938) 309-319.

[37] P. Kowalczyk, P. A. Gauden, A. P. Terzyk, A. V. Neimark, Screening of carbonaceous nanoporous materials for capture of nerve agents, Phys. Chem. Chem. Phys. 15 (2013) 291-298.

[38] A. V. Neimark, Y. Lin, P. I. Ravikovitch, M. Thommes, Quenched solid density functional theory and pore size analysis of micro-mesoporous carbons, Carbon 47 (2009) 1617-1628.

[39] J. Biscoe, B. E. Warren, An X-ray study of carbon black. J. Appl. Phys. 13 (1942) 364-371.

[40] A. P. Terzyk, G. Rychlicki, Adsorption of biologically active compounds from aqueous solutions on to commercial unmodified activated carbons. Part V. The mechanism of the physical and chemical adsorption of phenol, Coll. & Surf. A: Physicochem. Eng. Aspects 163 (2000) 135-141.

[41] M. Wiśniewski, A. P. Terzyk, P. A. Gauden, K. Kaneko, Y. Y. Hattori, Removal of internal caps during hydrothermal treatment of bamboo-like carbon nanotubes and application of tubes in phenol adsorption, J. Coll. Interface Sci. 381 (2012) 36-42.

[42] R. Saito, A. Jorio, A. G. Souza Filho, G. Dresselhaus, M. S. Dresselhaus, M. A. Pimenta, Probing phonon dispersion relations of graphite by double resonance Raman scattering, Phys. Rev. Lett. 88 (2001) 027401.

[43] M. S. Dresselhaus, A. Jorio, A. G. Souza Filho, R. Saito, Defect characterization in graphene and carbon nanotubes using Raman spectroscopy, Philos. Trans. R Soc. A 368 (2010) 5355-5377.

[44] A. Burian, A. Ratuszna, J. C. Dore, Radial distribution function analysis of the structure of activated carbons, Carbon 36 (1998) 1613-1621.

[45] M. Ruike, T. Kasu, J. N. Setoyama, T. Suzuki, K. Kaneko, Inaccessible pore

characterization of less-crystalline microporous solids, J. Phys. Chem. 98 (1994) 9594-9600.

[46] J. C. Dore, M. Sliwinski, A. Burian, W. S. Howells, D. Cazorla, Structural studies of activated carbons by pulsed neutron diffraction, J. Phys.: Condens. Matter 11 (1999) 9189-9201.

[47] W. A. Steele, The physical interaction of gases with crystalline solids: I. Gas-solid energies and properties of isolated adsorbed atoms, Surf. Sci. 36 (1973) 317-352.

[48] Ch. Lastoskie, K. E. Gubbins, N. Quirke, Pore size heterogeneity and the carbon slit pore: a density functional theory model, Langmuir 9 (1993) 2693-2702.

[49] P. I. Ravikovitch, A. Vishnyakov, R. Russo, A. V. Neimark, Unified approach to pore size characterization of microporous carbonaceous materials from N_2, Ar, and CO_2 adsorption isotherms, Langmuir 16 (2000) 2311-2320.

[50] M. Wiśniewski, S. Furmaniak, A. P. Terzyk, P. A. Gauden, P. Kowalczyk, Properties of phenol confined in realistic carbon micropore model: experiment and simulation, J. Phys. Chem. C 119 (2015) 19987-19995.

[51] C. H. Giles, T. H. MacEwan, S. N. Nakhwa, D. Smith, Studies in adsorption. Part XI. A system of classification of solution adsorption isotherms, and its use in diagnosis of adsorption mechanisms and in measurement of specific surface areas of solids, J. Chem. Soc. 1 (1960) 3973-3993.

[52] P. A. Gauden, A. P. Terzyk, P. Kowalczyk, G. L. Aranovich, M. Donohue, M. Ćwiertnia et al., G. Giles' classification of solute adsorption isotherms for binary non-electrolyte solutions via lattice DFT supported by experimental sorption data from aqueous solutions on carbonaceous materials, in Carbon Materials - Theory and Practice, A. P. Terzyk, P. A. Gauden, P. Kowalczyk, editors, Kerala: Research Signpost, 2008, p. 517-570.

[53] S. C. McGrother, K. E. Gubbins, Constant pressure Gibbs ensemble Monte Carlo simulations of adsorption into narrow pores, Mol. Phys. 97 (1999) 955-965.

[54] P. Kowalczyk, P. A. Gauden, A. P. Terzyk, E. Pantatosaki, G. K. Papadopoulos, Constant pressure path integral Gibbs ensemble Monte Carlo method, J. Chem. Theory and Comput. 9 (2013) 2922-2929.

[55] J. Landers, G. Y. Gor, A. V. Neimark, Density functional theory methods for characterization of porous materials, Coll. & Surf. A: Physicochem. Eng. Aspects 437

(2013) 3-32.

[56] J. Jagiello, Stable numerical solution of the adsorption integral equation using splines, Langmuir 10 (1994) 2778-2785.

[57] G. M. Davies, N. A. Seaton, Development and validation of pore structure models for adsorption in activated carbons, Langmuir 15 (1999) 6263-6276.

[58] S. H. Lin, R. S. Juang, Adsorption of phenol and its derivatives from water using synthetic resins and low-cost natural adsorbents: A review, Journal of Environ. Manage. 90 (2009) 1336-1349.

[59] W. Humphrey, A. Dalke, K. Schulten, VMD - Visual Molecular Dynamics, J. Molec. Graphics 14.1. (1996) 33-38.

[60] Z. Király, I. Dékány, E. Klumpp, H. Lewandowski, H. D. Narres, M. J. Schwuger, Selective sorption of phenol and related compounds from aqueous solutions onto graphitized carbon black. Adsorption and flow microcalorimetric studies, Langmuir 12 (1996) 423-430.

[61] R. J. L. Andon, J. F. Counsell, E. F. G. Herington, J. F. Martin, Thermodynamic properties of organic oxygen compounds, Trans. Faraday Soc. 59 (1963) 830-835.